Supplementary Information

Cell swelling, softening and invasion in a 3D breast cancer model

Author: Yu Long Han[1], Adrian F. Pegoraro[2,3], Hui Li[4,5], Kaifu Li[6], Yuan Yuan[3], Guoqiang Xu[1], Zichen Gu[1], Jiawei Sun[1], Yukun Hao[1], Satish Kumar Gupta[1], Yiwei Li[1], Wenhui Tang[1], Xiao Tang[6], Lianghong Teng[6], Jeffrey J. Fredberg[7] and Ming Guo[1*]

Affiliations:

1. Department of Mechanical Engineering, Massachusetts Institute of Technology, Cambridge, MA, 02139, USA;

2. Department of Physics, University of Ottawa, Ottawa, ON, K1N 6N5, Canada;

3. Harvard John A. Paulson School of Engineering and Applied Sciences, Cambridge, MA, 02138, USA;

4. School of Systems Science, Beijing Normal University, Beijing 100875, P.R. China;

5. National Laboratory for Condensed Matter Physics and Key Laboratory of Soft Matter Physics, Institute of Physics, Chinese Academy of Sciences, Beijing 100190, P.R. China;

6. Xuanwu Hospital, Capital Medical University, Beijing, 100053, P.R. China;

7. Harvard T. H. Chan School of Public Health, Boston, MA, 02115, USA;

[*]**Correspondence**:
Ming Guo
Massachusetts Institute of Technology, Cambridge, MA 02139, USA.
Phone: +1 (617) 324-0136
Email: guom@mit.edu

Supplementary Tables

Table S 1 Mechanical testing of hydrogels

Hydrogels	**Shear modulus (Pa)**
Matrigel (soft, 5 mg/mL)	30 ± 9
Alginate/Matrigel (5 mg/mL alginate and 4 mg/mL Matrigel, 20mM Ca^{2+})	349 ± 37
Collagen/Matrigel (3.5 mg/mL collagen with 0.5 mg/mL Matrigel)	330 ± 56

Supplementary Figures

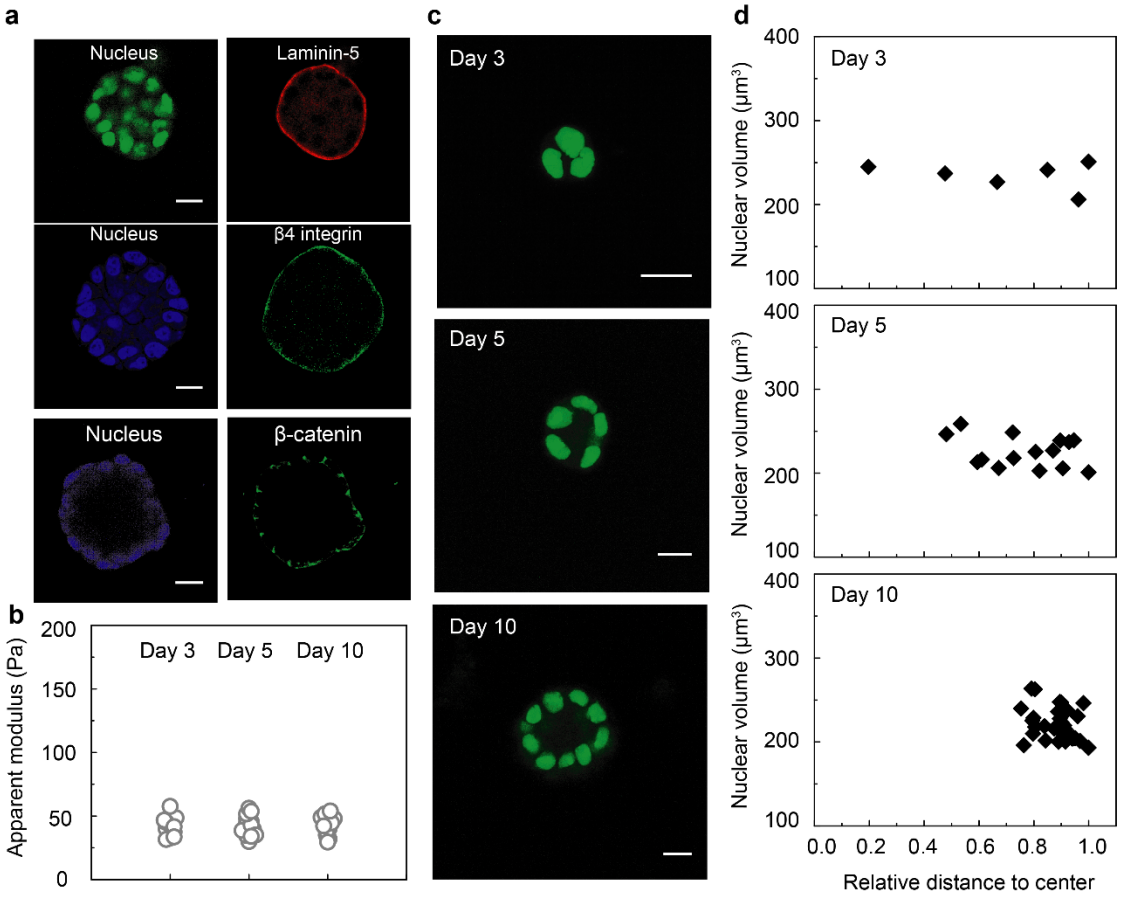

Figure S1. Temporal and spatial evolution of cell volume and mechanics during the growth of acinar structures of MCF10A cell line in 5 mg/mL Matrigel. a, Immunofluorescence images of the indicated components. **b**, Mechanical heterogeneity of individual cells within the acinar structure at different days. **c**, Time series of a MCF10A acinar structure growing in Matrigel from day 3 to day 10. **d**, Nuclear volume of every individual cell in the acinar structure is plotted against relative distance to the acinar center at different stages, showing no correlation between nuclear volume and spatial position. Scale bars: 20 μm.

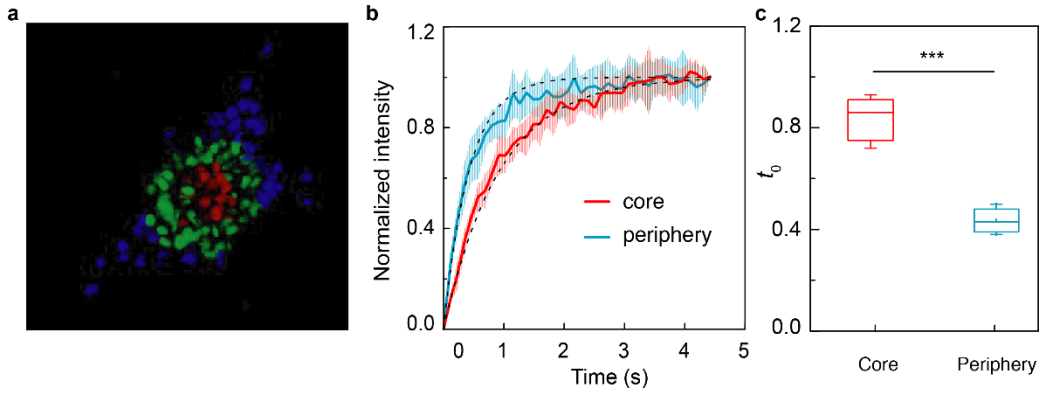

Figure S2. a, A section of a cancer organoid with different regimes labeled in different colors, i.e., core (red), periphery (green) and branch (blue). **b**, Fluorescence recovery after photobleaching (FRAP) of GFP-NLS in cell nucleus in periphery area (blue) and core area (red) of the organoid. In both areas, fluorescence recovered quickly after photobleaching but the rate of recovery was decreased significantly in the core area as compared to the periphery area. These curves are the average of 20 measurements, and error bars indicate the standard deviation. **c**, Characteristic time scale, t_0, from fitting the curves in b with $y(t) = 1 - e^{-\frac{t}{t0}}$, according to a recent protocol[1].

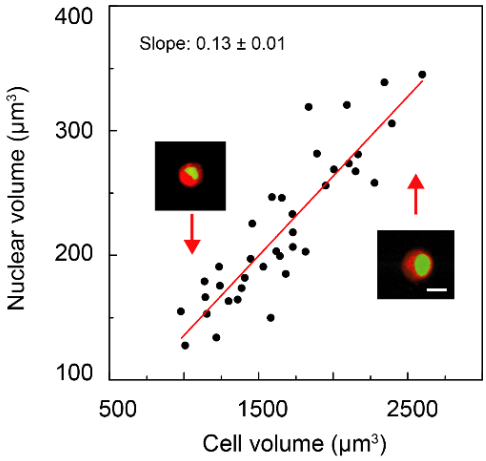

Figure S3. **The relationship between cell volume and nuclear volume in 3D cancer organoids**. Nuclear volume is plotted against cell volume of single cells within the 3D spheroid. Pearson correlation coefficient: 0.89. Insets: Representative images of cells with increasing cell volume. Scale bar: 10 μm.

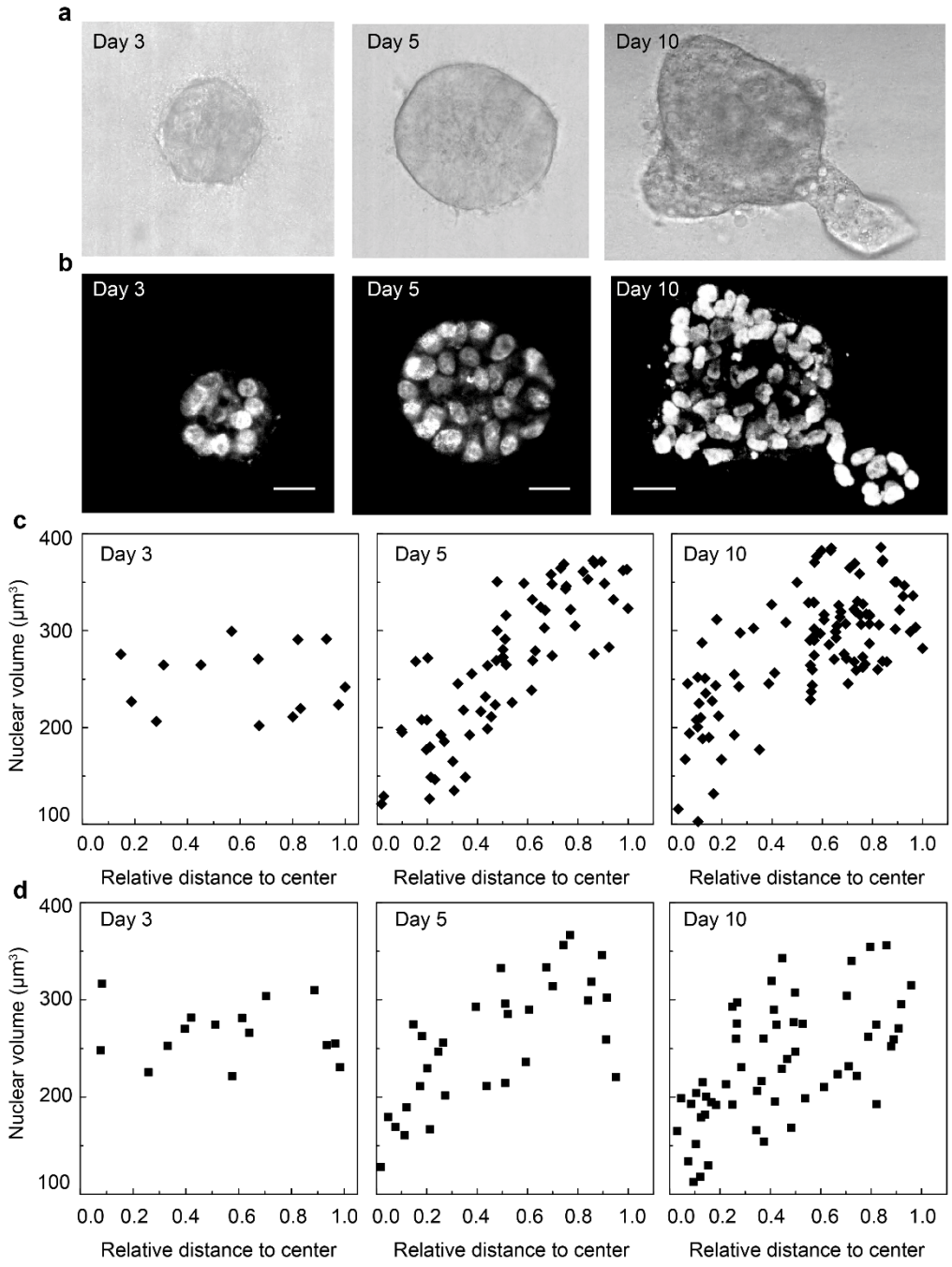

Figure S4. Temporal and spatial evolution of cell volume during the growth of premalignant MCF10AT cell line and normal MCF10A cell line in collagen/Matrigel hydrogel. a-b, Time series of a MCF10AT cancer spheroid growing from day 3 to 10. **c**, Nuclear volume of every individual cell in MCF10AT cancer organoid is plotted against relative distance to the cluster center at different stages, showing a strong correlation between nuclear volume and spatial position, particularly at middle and later stage. **d**, Nuclear volume of every individual cell in MCF10A cancer organoid is plotted against relative distance to the cluster center at different stages, showing a strong correlation between nuclear volume and spatial position, particularly at middle and later stage. Scale bar: 20 μm.

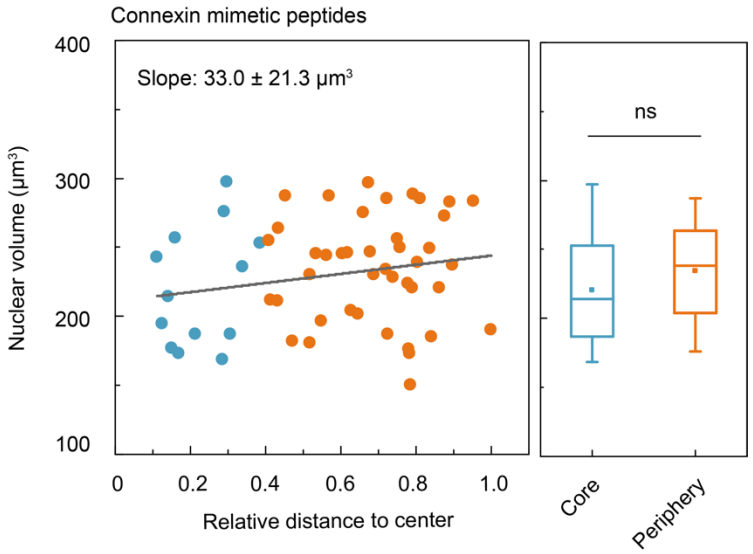

Figure S5. Connexin mimetic peptides (CMPs) specifically inhibit gap junctional communication and delay the formation of volume gradient in cancer organoid, suggesting that gap junctions play a role in the evolution of volume heterogeneity in cancer development.

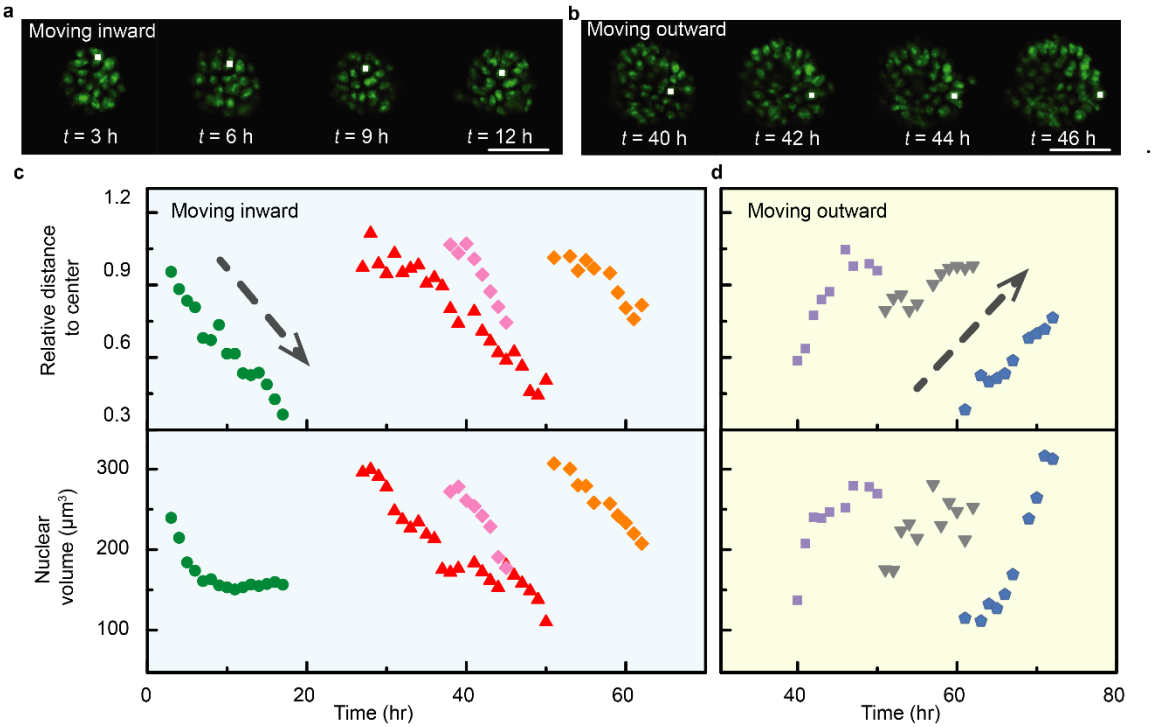

Figure S6. Individual cell physical properties are correlated with their location. a-b, Time-lapse images show an individual cell moves from the periphery to the core of the cancer organoids (a) and vice versa (b). **c-d**, Corresponding relative distance and volume changes of migrating cells in a growing cancer organoid are plotted against time. Cells migrating into the core and out to the periphery are shown in **c** and **d** respectively. Scale bars in **a** and **b** represent 50 μm.

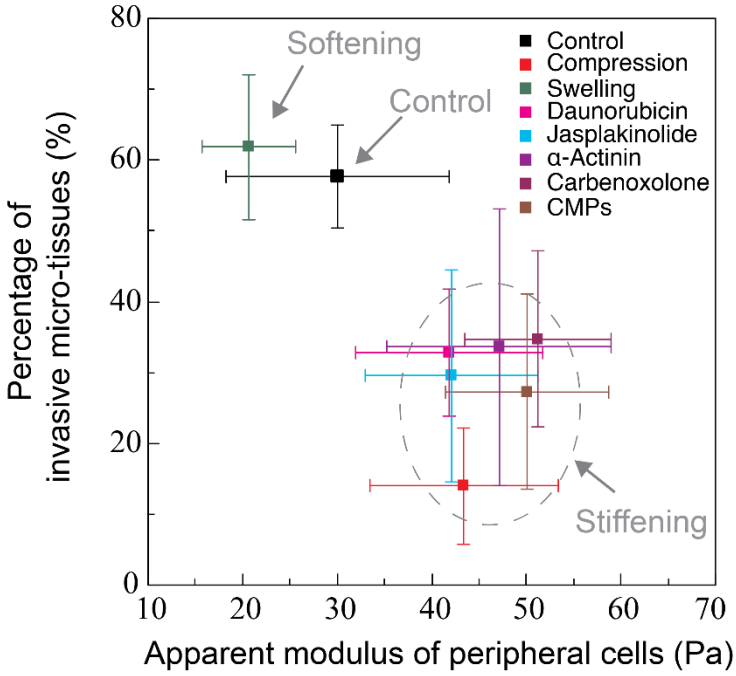

Fig. S7. The percentage of the invasive cancer spheroids is plotted against the apparent modulus of the peripheral cells, suggesting that the decrease or increase in cell stiffness was accompanied by a corresponding increase or decrease in the percentage of invasive cancer spheroids. CMPs represents treatment with connexin memetic peptides.

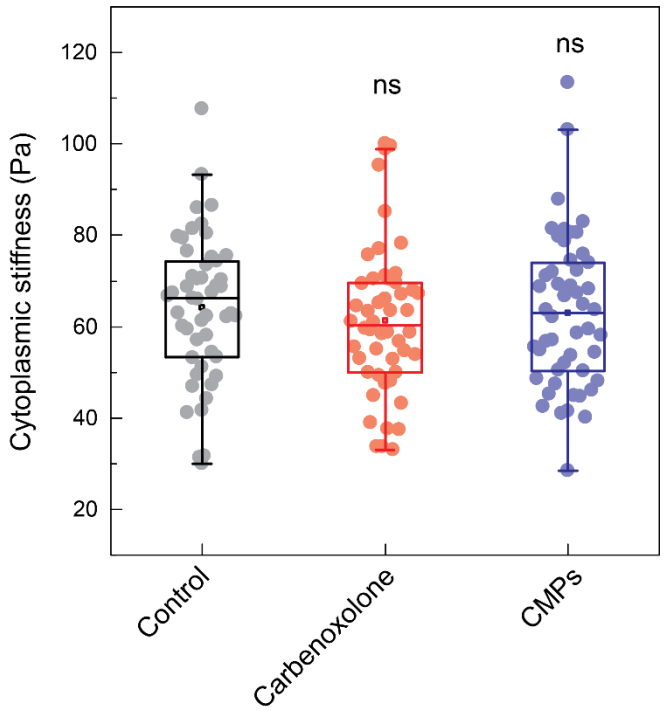

Fig. S8. The effect of gap junction (GJ) inhibitors on cell mechanics. To test whether GJ inhibitors (namely carbenoxolone and connexin mimetic peptides (CMPs)) would affect cells stiffness of isolated MCF10A cells in 2D culture, MCF10A cells were seeded on a 2D surface with a low cell density. After attachment, cells were treated with either carbenoxolone (100 μM) or CMPs (100 μM) for six hours. Then the cell mechanics were probed with optical tweezers, as described previously[2]. These results confirm that both GJ inhibitors we used do not change the cytoplasmic stiffness of isolated MCF10A cells in 2D culture.

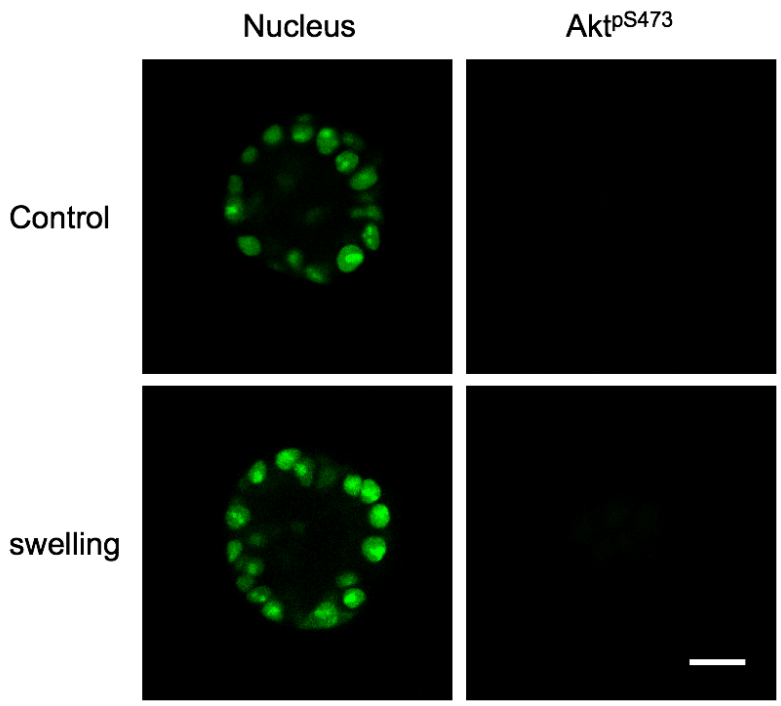

Figure S9. Immunofluorescence images of Akt^{pS473} from acinar structures formed by MCF10A cell line in 5 mg/mL Matrigel under normal condition and osmotic swelling. Scale bar: 20 μm.

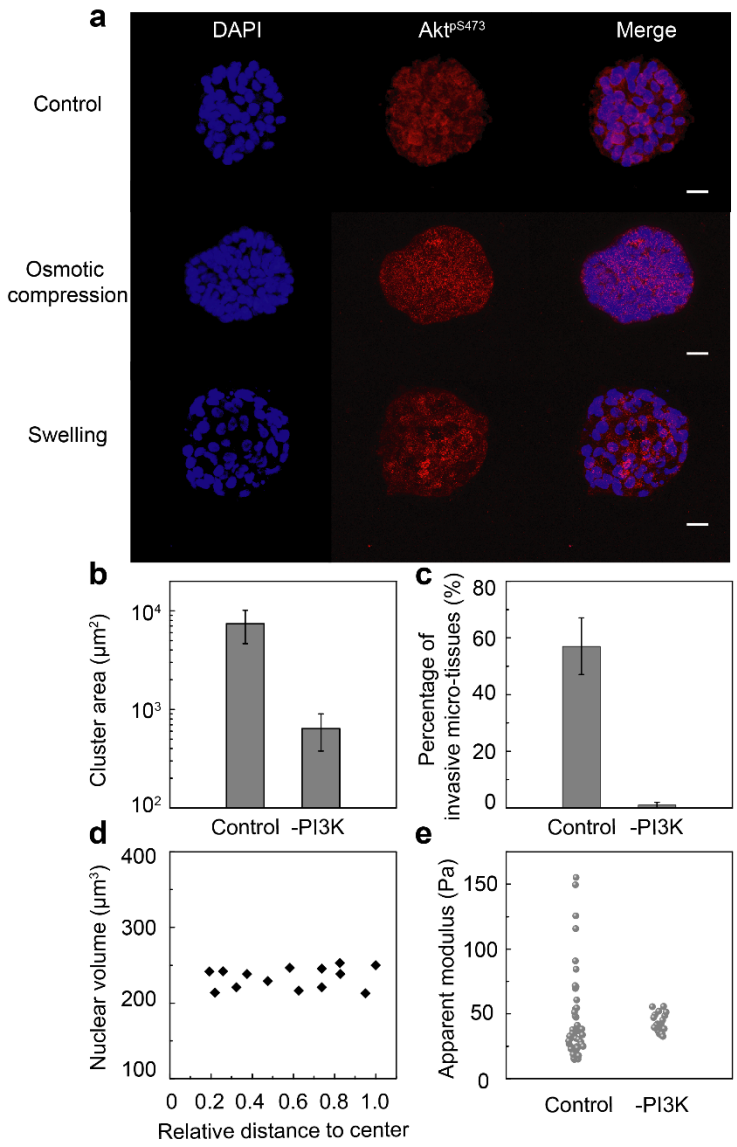

Figure S10. **a,** Immunofluorescent staining of Akt^{pS473} for cancer organoid under osmotic treatment. **b-e,** Growth area (b), invasiveness (c), nuclear volume (d) and cell stiffness (e) of cancer organoids on day 10 after PI3K pathway was inhibited with LY294002. Scale bar: 20 μm. To test the role of the PI3K pathway, we used 20 μM of the PI3K inhibitor LY294002 on MCF10A clusters on day 3 and performed the measurements on day 10. We found that the inhibition of PI3K significantly reduced the size of the cluster and the percentage of invasive clusters, as shown in Fig. S10b-c. Volume and stiffness measurements showed that there were no changes in cell volume and stiffness across the cluster when PI3K was inhibited (Fig. S10d-e). This is consistent with our hypothesis that the observed stiffness gradient in the control group is caused by the intratumor stress; when PI3K is inhibited, clusters remain small and thus intratumor stress must also remain small, precluding the development of a stiffness gradient. These results suggest that PI3K activation is required for MCF10A clusters to develop a mechanical gradient.

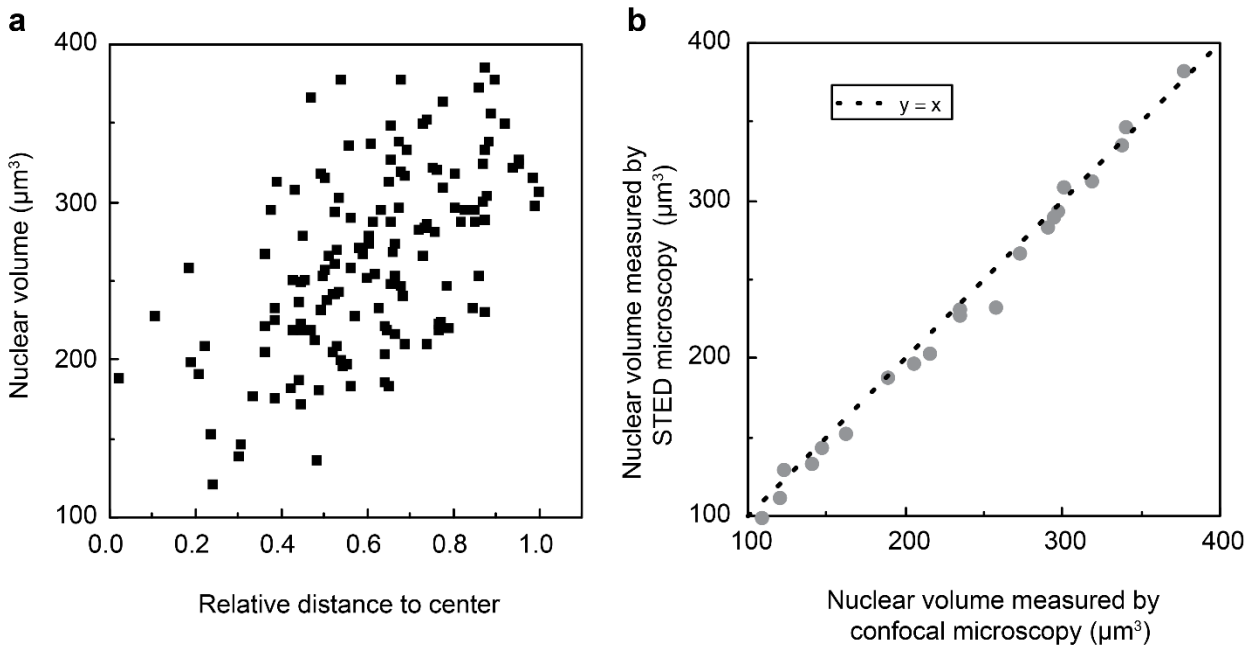

Figure S11. Comparison of the volume measurements using stimulated emission depletion (STED) microscopy in a superresolution mode with isotropic resolution in *x*, *y* and *z*, and laser scanning confocal microscopy. **a**, Nuclear volume of every individual cell in MCF10A cancer organoid is plotted against relative distance to the acinar center, which is consistent with the results measured by confocal microscopy. **b**, Nuclear volume of single cells is measured by STED and confocal microscopy, showing consistency between two methods.

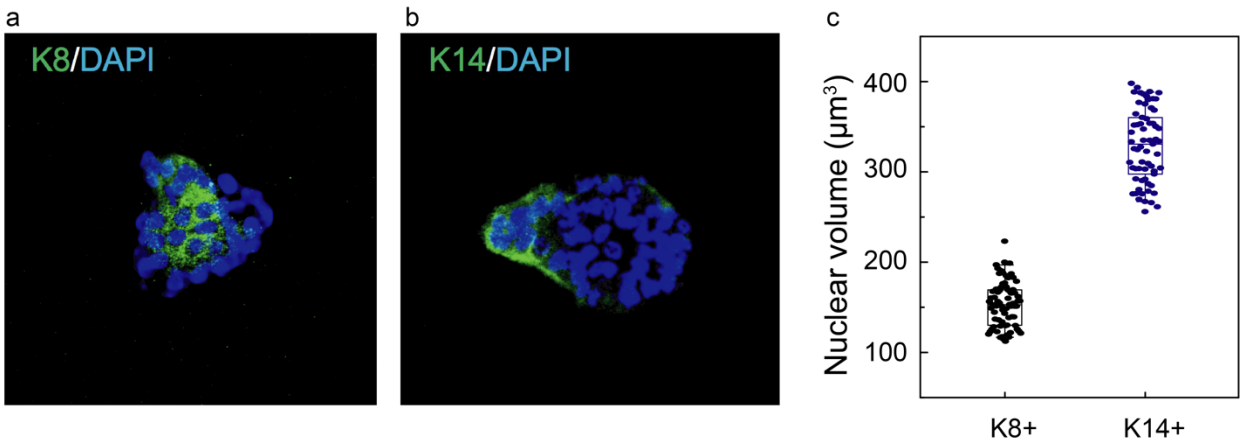

Figure S12. **a-b**, Immunofluorescence images of the indicated components from invasive micro-tissues formed by MCF10A cell line in collagen/Matrigel hydrogel. **c**, Cell nuclear volume of two cell populations that are positive for K8 and K14, respectively.

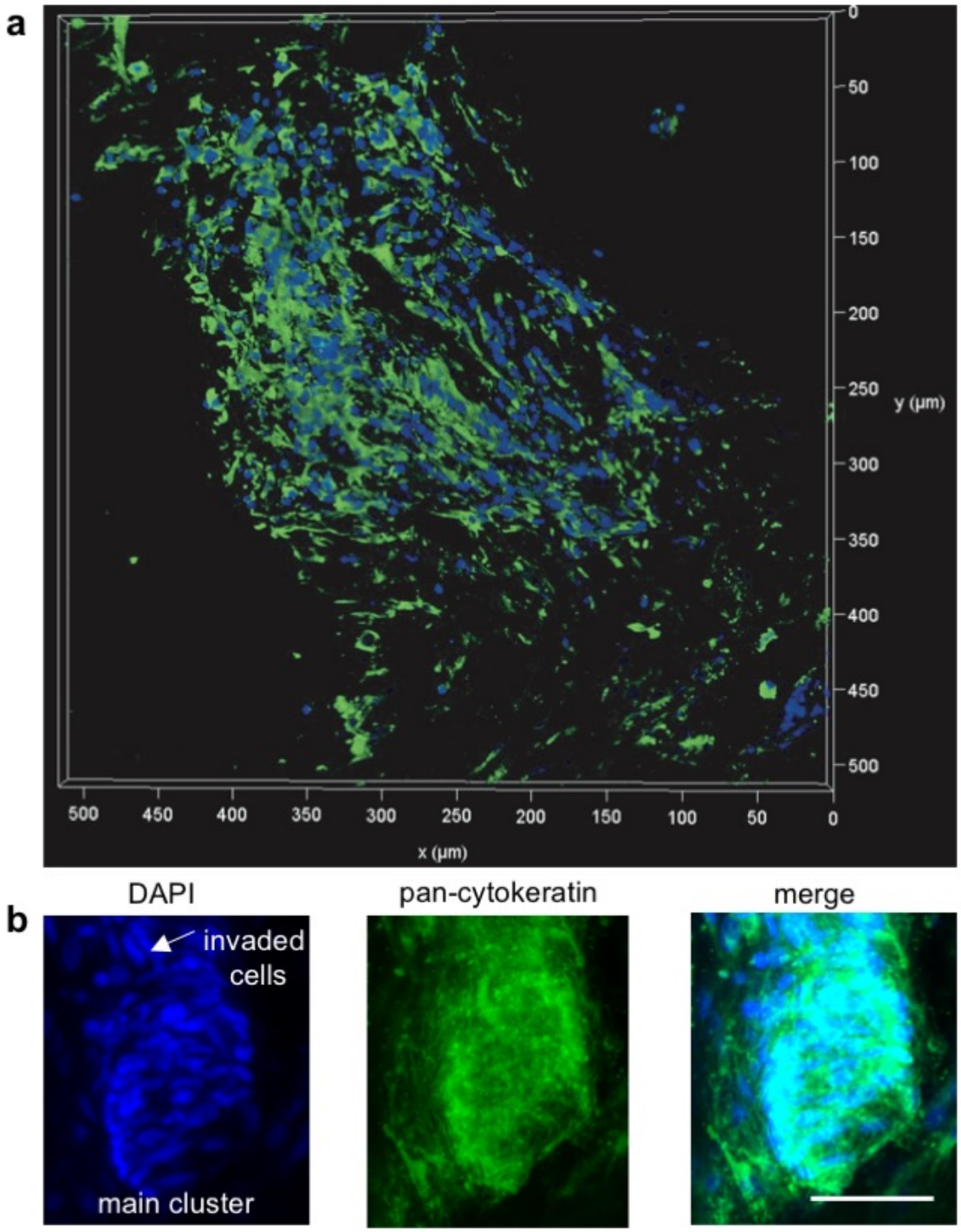

Figure S13. Immunofluorescent staining of a pan-cytokeratin (green) and cell nuclei (blue). Scale bar: 50 µm.

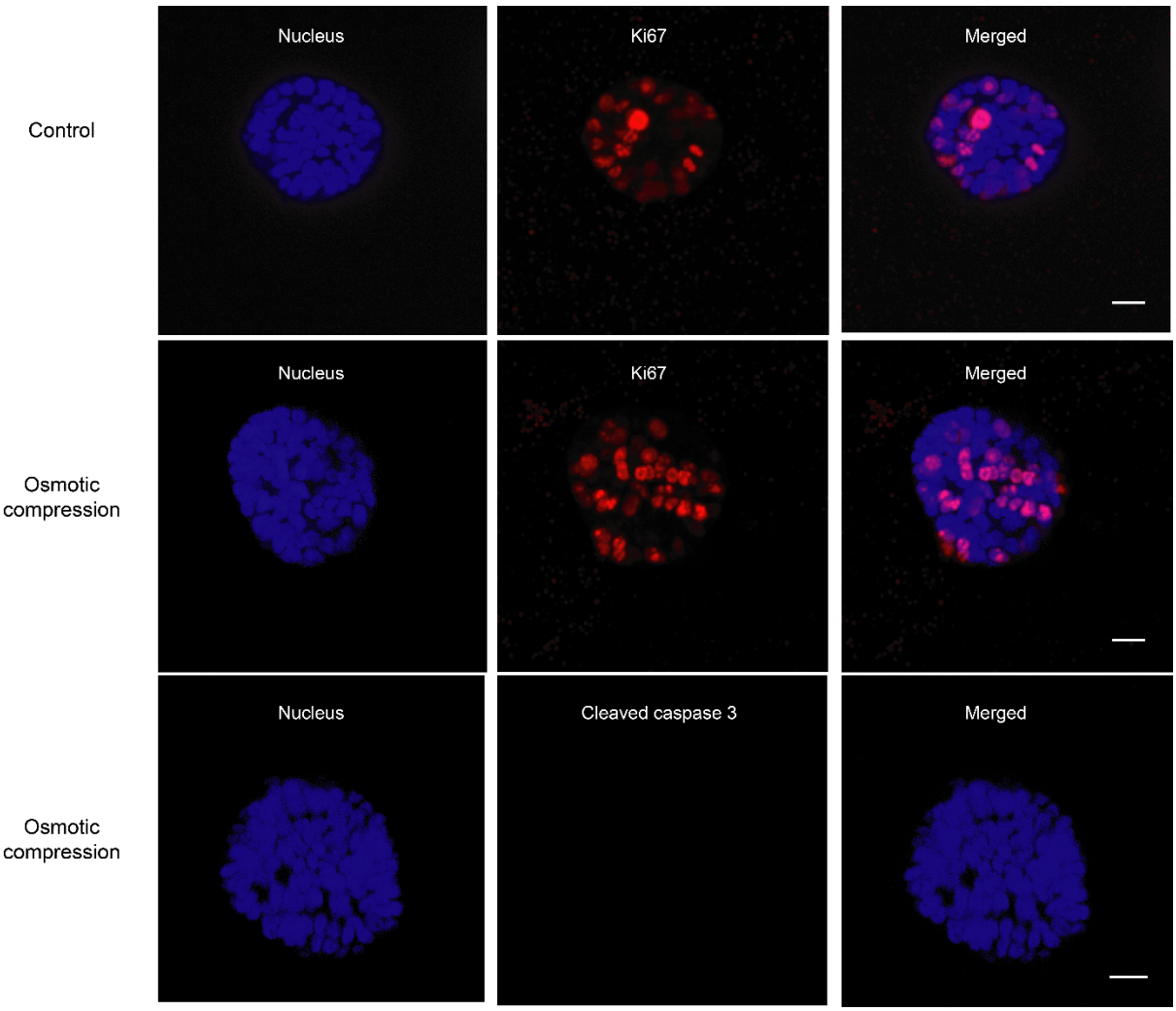

Figure S14. Immunofluorescent staining of a Ki67 and cleaved caspase 3 for cancer organoid under osmotic compression. Scale bar: 20 μm.

Captions for Supplementary Movies

Supplementary Movie 1. Middle stage tumor micro-dynamics before transitioning to an invasive behavior.

Supplementary Movie 2. Later stage tumor micro-dynamics after transitioning to an invasive behavior.

Supplementary Movie 3. Confocal images of malignant acini from grade-2 ER+ human invasive-ductal-carcinoma samples.

References:

1 Fritzsche, M. & Charras, G. Dissecting protein reaction dynamics in living cells by fluorescence recovery after photobleaching. *Nat. Protoc.* **10**, 660 (2015).

2 Hu, J. *et al.* Size- and speed-dependent mechanical behavior in living mammalian cytoplasm. *PNAS* **114**, 9529-9534 (2017).